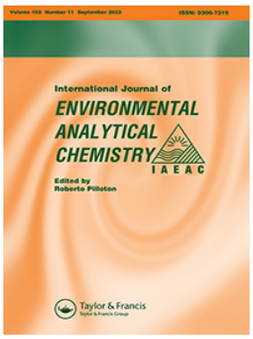

International Journal of Environmental Analytical Chemistry

ISSN: (Print) (Online) Journal homepage: https://www.tandfonline.com/loi/geac20

Adsorption, oxidation, kinetic and thermodynamic studies of methyl orange by magnetic Fe_3O_4 NPs and their chitosan/alginate nanocomposites

Muradiye Şahin, Yasin Arslan & Fatma Tomul

To cite this article: Muradiye Şahin, Yasin Arslan & Fatma Tomul (2022): Adsorption, oxidation, kinetic and thermodynamic studies of methyl orange by magnetic Fe_3O_4 NPs and their chitosan/alginate nanocomposites, International Journal of Environmental Analytical Chemistry, DOI: 10.1080/03067319.2022.2140417

To link to this article: https://doi.org/10.1080/03067319.2022.2140417

Published online: 02 Nov 2022.

INTERNATIONAL JOURNAL OF ENVIRONMENTAL ANALYTICAL CHEMISTRY
https://doi.org/10.1080/03067319.2022.2140417

Adsorption, oxidation, kinetic and thermodynamic studies of methyl orange by magnetic Fe_3O_4 NPs and their chitosan/alginate nanocomposites

Muradiye Şahin [a], Yasin Arslan [b] and Fatma Tomul [c]

[a]Chemistry Department, Institute of Science, Kırşehir Ahi Evran University, Kırşehir, Turkey; [b]Nanoscience and Nanotechnology Department, Faculty of Arts and Science, Burdur Mehmet Akif Ersoy University, Burdur, Turkey; [c]Chemistry Department, Faculty of Arts and Science, Burdur Mehmet Akif Ersoy University, Burdur, Turkey

ABSTRACT

Magnetic iron oxide (Fe_3O_4) nanoparticles, iron oxide chitosan (Fe_3O_4-CS) and iron oxide alginate (Fe_3O_4-AT) nanocomposite beads were synthesised using green synthesis method. They were used as both adsorbents for the adsorption of methyl orange (MO) dye from the wastewater and heterogeneous catalysts for the catalytic wet peroxidation (CWPO) of MO. While the dye removal was successfully performed with Fe_3O_4NPs, Fe_3O_4-CS and Fe_3O_4-AT in both adsorption studies and CWPO, the highest removal efficiency (99%) in the shortest time (8 min for adsorption, 20 min for CPWO) was obtained with Fe_3O_4-CS for MO removal. The adsorption experiments were performed with the batch techniques at different contact time, pH, initial dye concentration, temperature, amount of adsorbent and foreign ion effect parameters by Fe_3O_4-CS adsorbent. The equilibrium was quickly reached after 30 min at pH 3 and 298 K. Fitting equilibrium data to Langmuir, Temkin and Freundlich isotherms showed that Langmuir model was more suitable to describe MO adsorption with a maximum monolayer adsorption capacity of 132 mg/g at 298 K. The Experimental data were analysed using intra particle diffusion, pseudo-first-order and pseudo-second-order kinetic models and it was found that the adsorption kinetics followed a pseudo-second-order equation. Based on thermodynamic studies, adsorption process occurred as spontaneous and exothermic. The effects of the amount of catalyst, pH, temperature and H_2O_2 concentration were investigated to determine their catalytic activities for the decomposition of MO with CWPO technique. The reusability of Fe_3O_4-CS for both adsorption and CWPO techniques for MO removal was performed, and the adsorption and oxidation efficiency was found to be 97%. Moreover, the reaction kinetics was also investigated and the oxidation reaction was in good agreement with the pseudo-first order kinetic model. The activation energy (Ea) of the reaction was found to be 10.72 kJ/mol.

ARTICLE HISTORY
Received 26 July 2022
Accepted 20 October 2022

KEYWORDS
Adsorption; catalytic wet peroxidation; green synthesis; magnetic nanoparticles; methyl orange

1. Introduction

When the material size is reduced to the nanometre level, the changes in the interactions of the particles with each other and in the surface properties cause the emergence of new

CONTACT Yasin Arslan yasinarslan@mehmetakif.edu.tr

and superior properties in the structure which makes nano-structured materials increasingly used in the biotechnological, biomedical, optical and electronic applications [1–3]. In recent years, nanoparticles with magnetic properties have gained an important place among the nano-structured materials on which researches have focused on their use in the biotechnological and biomedical applications. The synthesis of magnetic nanoparticles can be done by many methods, such as co-precipitation [4–6], thermal cracking [7,8], hydrothermal synthesis [9,10], microemulsion [11] and green synthesis [12,13]. In this study, magnetic iron oxide (Fe_3O_4) nanoparticles were synthesised using an endemic plant, Lathyrus brachypterus, extract with a fast, economical, harmless to human health and environmentally friendly green synthesis method. This plant extract used as both reduction and stabilising agent for the synthesis of Fe_3O_4NPs. Dangerous and carcinogenic pollutants increasing as a result of developing industrialisation and rapid growth of existing production capacity cause widespread environmental pollution [14]. Many pollutants mix with many sources, such as air, water and soil. The dyeing process is an important step in the textile production and since dyes are used in many stages during the textile production, textile wastewater also contains a significant amount of these substances. Methyl Orange (MO) is an azo dyestuff; it is widely used in the textile, printing, paper, food and pharmaceutical industries and research laboratories, and its removal from water samples is extremely important due to its toxicity [15]. Azo dyes are xenobiotic compounds that are electron deficient due to the azo linkage (–N=N) and in many cases they have sulphonic (SO_3-) or other electron withdrawing groups that produce electron deficiencies and make the dye less susceptible to degradation by microorganisms. Among all dye types, azo dyes are the most commonly used dye in the worldwide with a production rate of 70% [16–19]. Azo dyes are harmful to living organisms as they are toxic and/or mutagenic. The presence of these dyes in the aquatic ecosystem causes the serious environmental and health problems [20]. When the dyestuffs are released into the environment after use, the waste materials that are mixed with the groundwater and prevent the use of drinking water and pose a threat to the ecosystem. Paint wastes tend to form a visible layer on the water surface due to their lower density than water, thus increasing turbidity. As a result, it prevents the entry of sunlight and respiration, which are needed by living things under water for photosynthesis and similar processes. The quality of the water gradually decreases, becoming a breeding ground for bacteria and viruses [21]. Chemicals found in paint waste discharged into water sources can evaporate into the environment and may cause shortness of breath or breathing problems upon inhalation. Moreover, dyes are also carcinogenic substances. As a result, water resources with paint waste pose a threat to all living things in its daily use or consumption. Therefore, treatment of wastewater from harmful dye waste is important to prevent their devastating effects on animals and humans [17]. An important application of magnetic nanoparticles is the removal of pollutants, such as heavy metals and dyes in aqueous media by adsorption [22,23]. In this study, the magnetic iron oxide (Fe_3O_4) nanoparticles were synthesized using endemic Lathyrus brachypterus plant extract with the green synthesis method and the magnetic iron oxide chitosan (Fe_3O_4-CS) and iron oxide alginate (Fe_3O_4-AT) nanocomposite functional beads were also synthesized using chitosan and alginate natural polymers. The kinetic and thermodynamic studies were carried out by using them in both MO adsorption and oxidation with CWPO technique. The synthesised nanoparticles and nanocomposites could be easily dispersed in the environment in which they

were applied and collected quickly with the help of a magnet in both adsorption and CWPO applications.

2. Experimental

2.1. Chemicals

Iron (II) sulphate heptahydrate ($FeSO_4.7\ H_2O$), iron (III) chloride hexahydrate ($FeCl_3.6\ H_2O$) hydrogen peroxide (H_2O_2), sodium hydroxide (NaOH) and chitosan were received from Sigma-Aldrich. Acetic acid (CH_3COOH), methyl orange ($C_{14}H_{14}N_3NaO_3S$) and sodium alginate ($C_6H_7O_6Na$) were received from Merck. Calcium chloride ($CaCl_2$) was received from Fluka. All solutions in the experimental studies were prepared with high-purity water (18 MΩ.cm) obtained from PURIS pure water system (PURIS, Expe-UP Series). All of the materials were in analytical reagent grade and utilised as received without any purification.

2.2. Instrumentation

The chemical and morphological characterisations for the nanoparticles were realised by Shimadzu UV-1800 (UV-Vis), Perkin Elmer Frontier model FT-IR, Bruker D8 Advance model X-ray diffraction (×RD) with a Cu K_α radiation source in 2θ range from 10° to 90°, TEM-120kV Transmission Electron Microscope (TEM) and Carl Zeiss EVO-LS 10 Scanning Electron Microscope (SEM), respectively. Common drift method [24] was used to determine the pH (pHpzc) of nanoparticles and nanocomposites at the zero charge point. For this, 50 mL of 0.01 M NaCl solution was placed in a closed Erlenmeyer flask. The pH value was adjusted to a value between 2.0 and 12.0 by adding 0.1 M HCl or 0.1 M NaOH solutions. Then 0.05 g of each nanoparticle/nanocomposite was added and the final pH was measured using the pH metre (Thermo Scientific, Orion 3 Star) after 24 h under shaking at room temperature. The intersection point between the initial pH and final pH values was determined as pHpzc.

2.3. Preparation of adsorbent and catalyst

2.3.1. Synthesis of Fe_3O_4NPs

One gram of *Lathyrus brachypterus* plant was gauged and mixed with 50 mL of distiled water. The mixture was stirred continuously at 25°C for 5 h and solid phase was separated with a filter paper to obtain *Lathyrus brachypterus* extract [25]. To synthesise Fe_3O_4NPs, 100 mL aqueous solution including 0.56 g $FeSO_4.7\ H_2O$ and 0.81 g $FeCl_3.6\ H_2O$ was prepared and then 10 mL of the plant extract was added to the above prepared solution. Then, it was mixed at room temperature for 30 min at 500 rpm with a magnetic stirrer and left to settle. The synthesised Fe_3O_4NPs were separated with a magnet and washed 3 times with distiled water and dried in an oven.

2.3.2. Synthesis of Fe_3O_4-CS

0.50 g of chitosan was mixed with 50 mL of 1% acetic acid until a homogeneous mixture was obtained. Then, 0.40 g of the synthesised magnetic Fe_3O_4NPs was added to this

mixture and dropped into 100 mL of 1 M NaOH solution with a dropper to form Fe_3O_4-CS beads. The formed beads were kept in NaOH for 12 h, washed with distiled water. At the end of the period, half of them were kept in distiled water at 4°C, and the other half was dried in an oven at 50°C to compare their adsorption effects separately.

2.3.3. Synthesis of Fe_3O_4-AT

0.60 g of sodium alginate was mixed with 50 mL of distiled water until a homogeneous solution was formed. 0.50 g Fe_3O_4NPs was added to the prepared mixture and sonicated for 30 min. Then, Fe_3O_4-AT beads were formed by dropping the obtained homogeneous solution into 2% of $CaCl_2$ solution. The obtained beads were washed with distiled water and stored into distiled water at 4°C.

2.4. Adsorption studies

The removal of MO from wastewater by adsorption on magnetic nanoparticles (Fe_3O_4NPs, Fe_3O_4-CS and Fe_3O_4-AT) using the batch adsorption method was investigated. For this, a stock solution of 1000 mg/L MO was prepared. Then, this solution was diluted to prepare all other MO standard solutions. In adsorption experiments, 50 mg adsorbent was contacted with 50 mL 25 mg/L MO solution in a 100 mL beaker. Afterwards, the concentration of them remaining without being adsorbed in the solution was determined by measuring the absorbances at 465 nm, which is the maximum absorbance wavelength of MO with a UV–vis spectrophotometer. According to experimental results, it was seen that the most suitable adsorbent was found to be Fe_3O_4-CS nanocomposite which adsorbed 99% of MO in 8 min, and optimisation studies were carried out with these magnetic nanocomposite beads. In order to provide the highest removal of MO adsorption on Fe_3O_4-CS, in the batch system, the effects of initial dye concentration, contact time, pH, temperature, amount of adsorbent and salt concentration on the adsorption capacity were investigated in detail. For pH adjustments, 0.1 M HCl and 0.1 M NaOH solutions were prepared and small volumes (1–2 drops) were used from these solutions. The total volume added to achieve the desired pH was also taken into account for calculating the initial concentration. All samples were mixed at 250 rpm. Adsorption kinetic studies were performed at 298 K for 2–60 min. Adsorption isotherm experiments were also performed at different temperatures (298, 313 and 328 K) for 60 min with initial concentrations ranged from 2.5 to 200 mg/L MO. Thermodynamic parameters for the adsorption reactions were also determined.

2.5. Catalytic wet peroxidation of methyl orange by H_2O_2 experiments

A stock solution of 100 mg/L MO was prepared. Then, this solution was diluted and a calibration plot was drawn by preparing MO standard solutions at 2, 4, 6, 8 and 10 mg/L concentrations. For CWPO experiments, 100 mL of MO solution at a concentration of 25 mg/L was mixed in a magnetic stirrer at 250 rpm. Oxidation experiments were carried out at pH = 5 at room temperature. The catalytic process was started by adding 3 mL of freshly prepared 30% of H_2O_2 and then 0.10 g of magnetic nanoparticle/nanocomposite catalyst was added to the solution and mixed for 30 min. Two millilitres of sample was taken at regular intervals, separated from the catalyst by magnet, and 2 mL of distiled water was added to it and UV-Vis. measurement was taken. The effects of the amount of

catalyst, pH, temperature and H_2O_2 concentration were investigated in order to determine their catalytic activities on the decomposition of MO with CWPO technique and both the reusability of the catalysts and the reaction kinetics were also investigated.

3. Results and discussion

3.1. Characterization

The Fe_3O_4NPs was characterised by UV-Vis., FT-IR, XRD, SEM-EDX and TEM. The UV–Vis spectroscopy is a generally used practice to determine the different metal nanoparticles [26]. Synthesis of Fe_3O_4NPs using endemic plant extract was first decided with the colour changes that a light green colour of watery solution gradually changed to black colour. Secondly, it was observed that the synthesised magnetic nanoparticles were attracted by the magnet from the aqueous solution and the characteristic peak of Fe_3O_4NPs was observed at 290 nm in the UV-Vis spectrometer (Figure 1). The pH_{PZC} values of Fe_3O_4NPs, Fe_3O_4-CS and Fe_3O_4-AT were found to be 6.47, 5.18 and 5.65, respectively (Figure 7(c)). The studies were carried out at pH 3, which is below the pzc value for all adsorbents.

FTIR spectra of Fe_3O_4NPs, CS, Fe_3O_4-CS and Fe_3O_4NPs, AT, Fe_3O_4-AT are comparatively given in Figures 2(a) 2 2(b), respectively. The characteristic peak was seen at 555 cm^{-1} in FT-IR spectra of all synthesised nanoparticles and nanocomposites. In the literature, it was explained that the absorption bands of Fe_3O_4 nanoparticles in FTIR spectrum are able to be observed in between 550 and 1650 cm^{-1} because of flexural vibrations of the Fe – O group [29–31]. The peak seen at 3365 cm^{-1} in the FT-IR spectrum of Fe_3O_4-CS belongs to the -NH or -OH asymmetric vibration of chitosan. The width of this peak is due to the presence of hydrogen bonding in the nanocomposite. An H bond is formed by connecting the -NH or -OH group of pure chitosan to the -OH group of acetic acid [32]. Apart from these, the stretching vibration of C=O at 1732 cm^{-1}, the C-O-C bonds of the

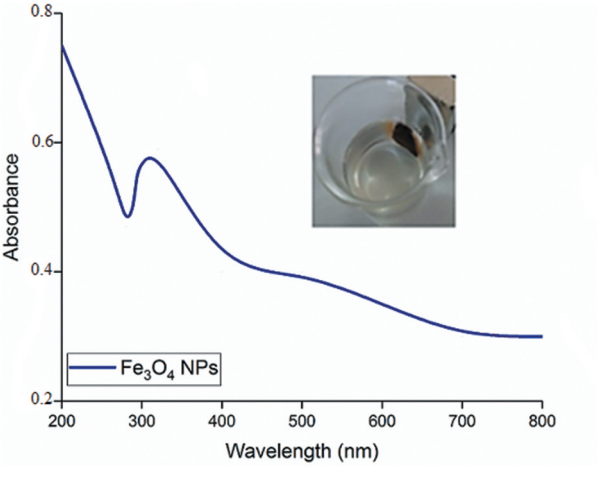

Figure 1 UV–vis spectra of Fe_3O_4NPs (conditions: plant extract volume 10 mL, 0.56 g $FeSO_4.7H_2O$, 0.81 g $FeCl_3.6H_2O$, 25 °C).

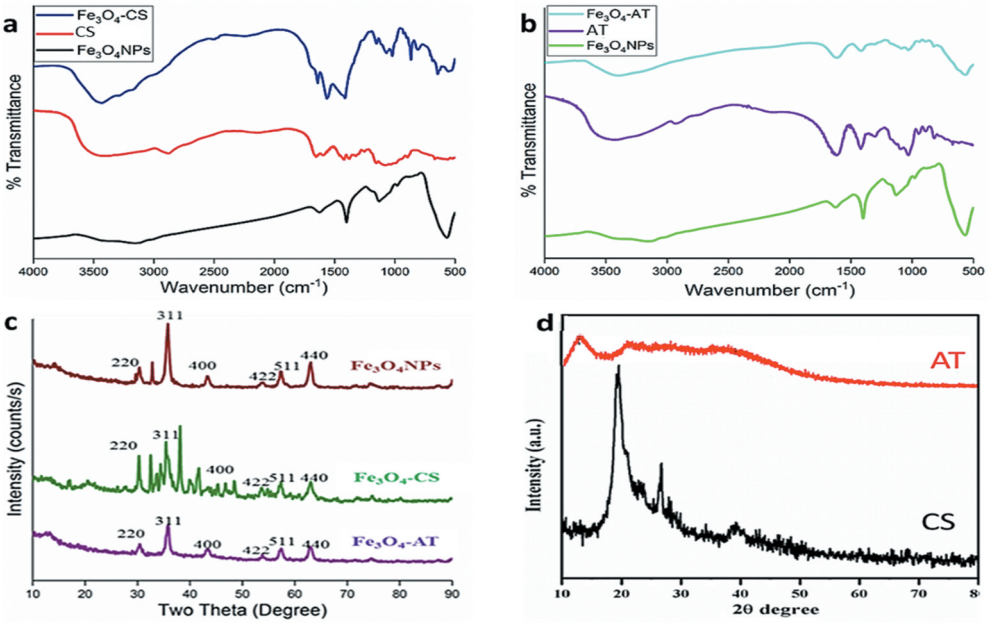

Figure 2. FTIR spectrum of a) Fe_3O_4NPs, CS, Fe_3O_4-CS b) Fe_3O_4NPs, AT, Fe_3O_4-AT and XRD pattern of c) Fe_3O_4NPs, Fe_3O_4-CS and Fe_3O_4-AT d) only CS [27] and AT [28]. .

polysaccharide skeleton at 1028 cm^{-1} and the characteristic peaks of β-1,4-glycosidic bond at 1153 and 895 cm^{-1} show that chitosan is present in the structure [33]. Furthermore, 3313 cm^{-1} O-H stresses, asymmetric and symmetrical stresses due to –COO at 1595 and 1417 cm^{-1}, -O-C-O- stretches of ether groups at 900–1200 cm^{-1} and –C-O- stretches seen in the FT-IR spectrum of Fe_3O_4-AT indicate that alginate is present in the structure [34–36].

The X-ray diffraction patterns of Fe_3O_4NPs, Fe_3O_4-CS and Fe_3O_4-AT magnetic nanoparticles are shown in Figure 2(c). In the XRD pattern of Fe_3O_4NPs, six peaks belonging to the crystal structures (220), (311), (400), (422), (511) and (440) were observed corresponding to the angle values of 2θ = 30.18°, 35.47°, 43.30°, 53.42°, 57.18° and 62.70° (JCPDS 65–3107), respectively. The particle size of a sample studied by XRD can be calculated using the half-width of the most intense peak in the diffraction pattern [37]. The crystal size of Fe_3O_4NPs was calculated to be 11.02 nm from the Debye-Scherrer equation (Equation 1) using the peak intensity observed at 2θ = 35.47° in the diffraction pattern of these nanoparticles. Six peaks detected in the XRD pattern of Fe_3O_4NPs were also detected in the diffraction pattern of Fe_3O_4-CS and Fe_3O_4-AT nanocomposites. The XRD of Fe_3O_4-CS showed a broad band around 20°. This result showed that the coating of Fe_3O_4NPs with chitosan and alginate did not change the crystalline structure of Fe_3O_4, thus did not change the spinel structure of Fe_3O_4 [38–40]. The crystal sizes of Fe_3O_4-CS and Fe_3O_4-AT nanocomposites were also calculated and found to be 12.02 and 13.52 nm, respectively, from the same equation, using the peak observed at 2θ = 35.47°, which has the maximum intensity in the diffraction pattern of these nanoparticles. In this case, the chitosan coating thickness on the surface was 1 nm and the alginate coating thickness was 1.5 nm.

$$D_{311} = \frac{k\lambda}{(\beta \cos\theta)} \tag{1}$$

where, D is crystallite size, k (0.891) is Debye-Scherrer's constant, λ (1.5406 A^{o}) stands for X-ray wavelength, β indicates the full width at half maximum intensity (*FWHM*) of the XRD peaks and θ is the difraction angle (*2θ)*.

The shape and size of the Fe_3O_4NPs were additionally characterised by TEM and SEM-EDX analysis (Figure 3). The SEM images show individualistic Fe_3O_4NPs besides a series of aggregates. The map data of elemental mapping confirmed the presence of Fe and O and is consistent with the SEM images (Figure 3(c)). The EDX spectra of Fe_3O_4NPs reveal that there are both Fe and O atoms in its structure (Figure 3(c)). TEM images (Figure 3(b)) obviously show that the nanoparticles are nearly spherical in shape. Figure 3(b) also indicates the size distribution histogram of the particles and while the sizes of the nanoparticles vary among 5 nm and 42 nm, the mean size of the particles is found to be 11.02 ± 0.15 nm. As seen, there is a good agreement with the particle sizes calculated by the Scherrer equation in the XRD pattern shown in Figure 2(c).

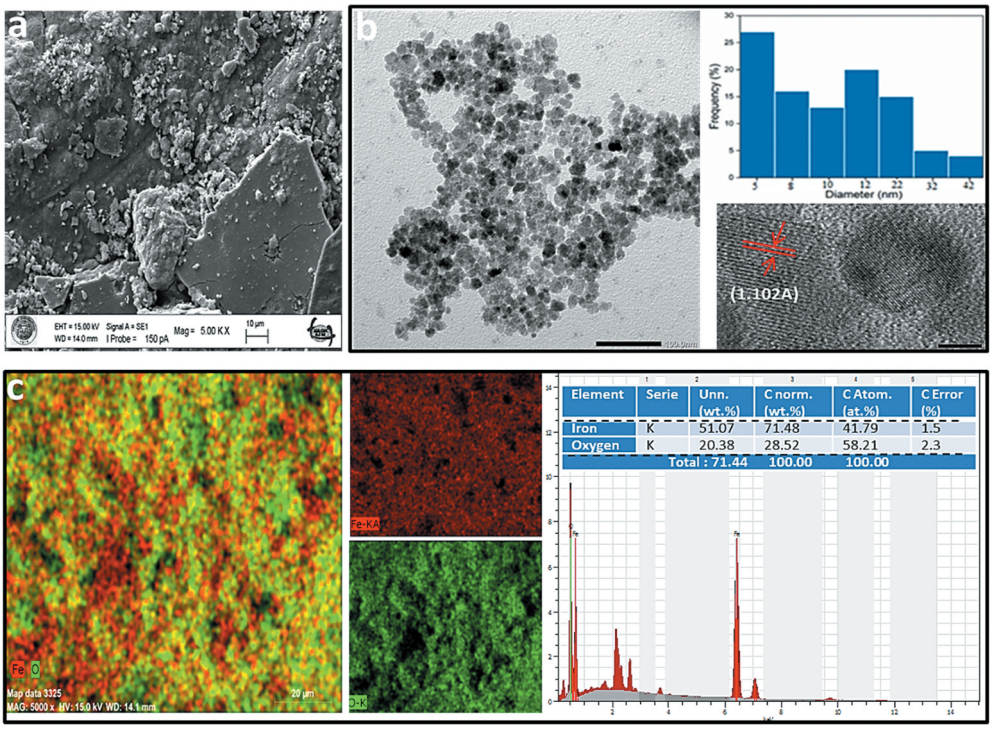

Figure 3. A) SEM images of Fe_3O_4NPs b) TEM, HR-TEM images and histograms of Fe_3O_4NPs c) Elemental mapping and EDX analysis of Fe_3O_4NPs.

3.2. Adsorption performances of MO onto magnetic adsorbent

The adsorption of 25 ppm of 50 mL MO on 50 mg of Fe_3O_4NPs, Fe_3O_4-CS and Fe_3O_4-AT magnetic nanoparticles at room temperature was separately investigated, and the results are given in Figure 4.

Optimisation studies were carried out with Fe_3O_4-CS, which showed the highest adsorption capacity in the shortest time. In addition, as described in the section 2.3.2, the adsorption effects of Fe_3O_4-CS beads stored in pure water at 4°C and dried in an oven at 50°C were also compared and it was seen that the one stored in water gave better results and in all further studies, those stored in pure water were used.

The amount of adsorbed dye, Q_e (mg/g), is calculated by Equation 2

$$Q_e = \frac{(C_0 - C_e)V}{W} \tag{2}$$

where C_0 and C_e are the initial and equilibrium concentrations (mg/L), respectively, V is the volume of dye solution (L), and W is the weight (g) of Fe_3O_4-CS adsorbent.

The FT-IR spectra of Fe_3O_4-CS for before and after adsorption of MO are comparatively given in Figure 5. The absorption bond seen at 3500 cm^{-1} of the O-H group in the Fe_3O_4-CS is shifted to lower wavenumber and narrowed after adsorption of MO. As seen in Figure 5, the peaks of – COO stretching within 1500–1600 cm^{-1} were disappeared after the MO dye is bound to the Fe_3O_4-CS surface [41].

3.2.1. Effect of initial dye concentration

The effect of the initial dye concentration on the adsorption amount and dye removal efficiency was investigated by changing the MO concentration in the range of 25–200 mg/L, and the results are given in Figure 6. As the initial concentration increased, the adsorption capacity increased, but the percentage of dye removal decreased. Higher removal efficiency at low MO concentration is associated with an increase in concentration gradient and analyte diffusion rate as a result of the availability of adsorbent sites

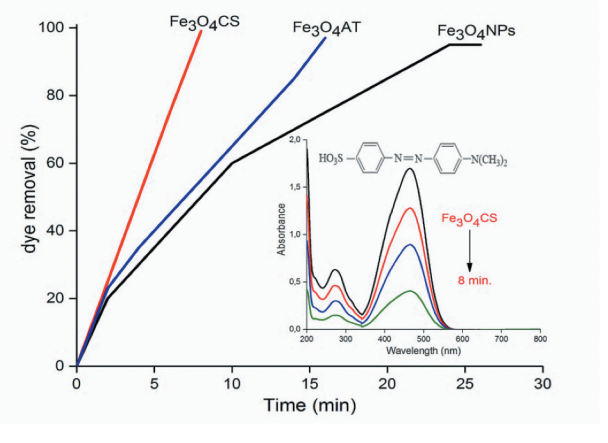

Figure 4. Comparative MO adsorption of Fe_3O_4NPs, Fe_3O_4-CS and Fe_3O_4-AT (initial dye concentration: 25 mg/L, adsorbent dosage: 50 mg/50 mL, T = 298 K).

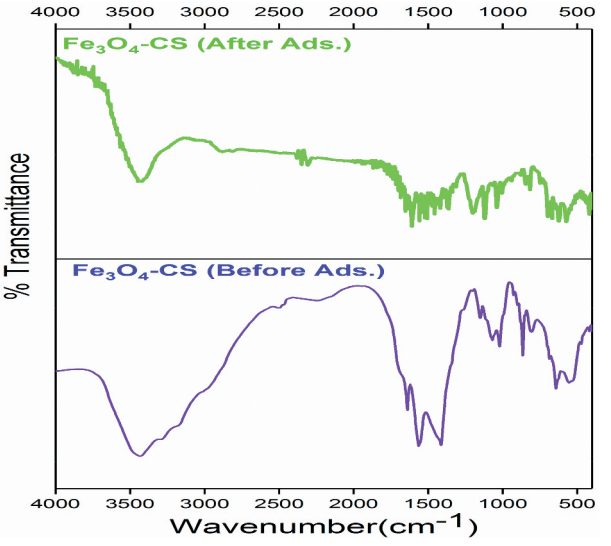

Figure 5. FTIR spectra of Fe_3O_4-CS for before and after adsorption of MO.

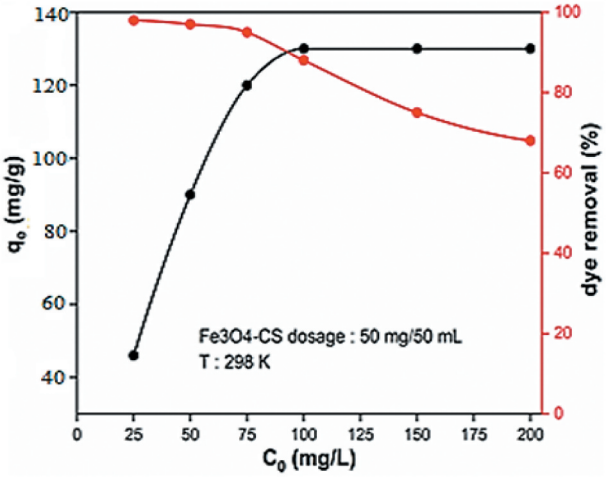

Figure 6. Effect of initial dye concentration on the removal of MO dye by Fe_3O_4-CS.

where dye ions can be adsorbed [42]. In addition, the presence of intraparticle diffusion at high dye concentrations causes the sorption to be slower [22]. Therefore, the subsequent experiments were carried out at a concentration of 50 mg/L, which gave better results in both adsorption amount and dye removal.

3.2.2. Effect of contact time

The variation of the amount of MO adsorbed on Fe_3O_4-CS beads at 2, 4, 6, 8, 10, 20, 30, 40, 50 and 60 min over time is given in Figure 7(a). The amount of MO adsorbed on Fe_3O_4-CS beads is increased among 0–30 min and did not change much after 30 min. Therefore, it can be said that the adsorption reaches equilibrium in 30 min. Therefore, all subsequent

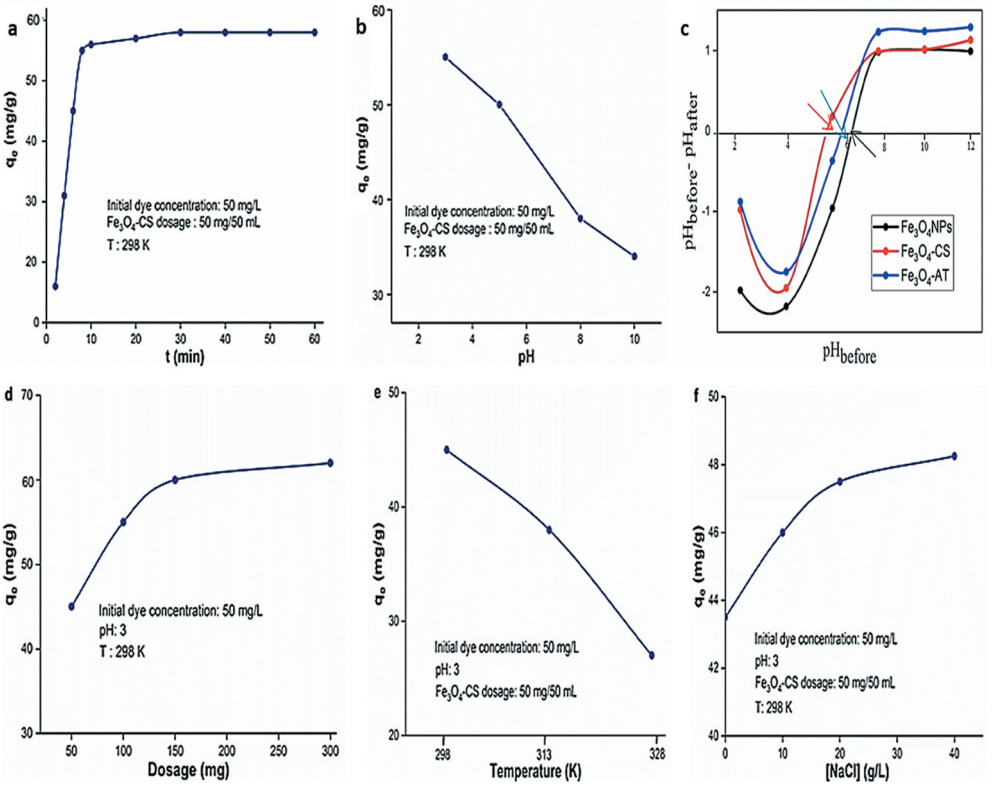

Figure 7. Effect of a) contact time, b) initial pH, c) point zero charge $pH_{pzc,}$ d) adsorbent dose, e) temperature and f) electrolyte concentration on the removal of MO dye by Fe_3O_4-CS.

experiments were carried out during this period and measurements were taken at the end of this period.

3.2.3. Effect of initial pH

The effect of pH for MO adsorption on Fe_3O_4-CS beads was investigated at pH 3, 5, 8 and 10 and the variation of qe values with pH is given in Figure 7(b). It was observed that the adsorption decreased with increasing pH. With the increase in pH, repulsive forces between – OH ions in the solution and – OH groups on the surface of iron oxide nanoparticles become effective and cause a decrease in MO adsorption on Fe_3O_4-CS. Fe_3O_4-CS beads showed maximum adsorption capacity at pH 3. In addition, as seen in Figure 7(c), pHpzc values of all adsorbents are above 3. At pH below the pHpzc value, higher hydrogen ion concentration, the negative charges at the surface of internal pores are neutralised and some more new adsorption sites were developed because the surface provided a positive charge for anionic MO dye to get adsorbed. A similar type of behaviour is also reported for the adsorption of the dye at different adsorbents [43–47].

3.2.4. Effect of adsorbent dose

The effect of the amount of adsorbent for the MO adsorption on Fe_3O_4-CS beads was investigated, and the variation of q_e values with the amount of adsorbent is given in

Figure 7(d). It was observed that the adsorption increased with the increase in the amount of adsorbent, but the amount of increase was in a decreasing acceleration over time. It is thought that this is due to the increase in the number of suitable areas where the dyestuff will be adsorbed as a result of the increase in the bonding points on the surface of the adsorbent, but at higher adsorbent doses, the surface area of the substance will decrease due to a possible aggregation. Maximum adsorption for MO was obtained by using 150 mg Fe_3O_4-CS adsorbent.

3.2.5. Effect of temperature

The effect of temperature for the MO adsorption on Fe_3O_4-CS beads was investigated at 298, 313 and 328 K, and the variation of q_e values with temperature is given in Figure 7(e). It was observed that the adsorption decreased with increasing temperature. This suggests that adsorption is controlled by an exothermic process.

3.2.6. Effect of supporting electrolyte (NaCl) concentration

In order to investigate the effect of ionic strength on adsorption capacity, solutions containing NaCl salt adjusted in different concentration ranges were prepared and the results are given in Figure 7(f). The increase in the amount of dye adsorbed with the increase of salt concentration can be explained by the decrease in the thickness of the electrical double layer due to the increase in the total number of ions in the adsorption medium, and thus the increase in the adsorption efficiency of the dyestuff anions [48].

3.3. Adsorption isotherms

In the study of dye adsorption, the three most commonly used adsorption isotherms are Langmuir, Freundlich and Temkin adsorption isotherms. According to the Langmuir isotherm, adsorption takes place in uniform energy regions on the adsorbent surface and does not go beyond the monolayer coating [49,50]. The Freundlich isotherm is an empirical equilibrium equation based on adsorption on a heterogeneous surface [5]. The Temkin isotherm reflects the indirect interactions between the adsorbent–adsorbate during the adsorption process and concludes that the heat of adsorption of all molecules in the layer decreases linearly due to these interactions. The graphs drawn according to the Langmuir (Equation 3), Freundlich (Equation 4) and Temkin (Equation 5) isotherms are given in Figure 8 based on the removal of MO from the aqueous medium with magnetic Fe_3O_4-CS beads. The parameters calculated from these graphs are also given in Table 1.

$$Q_e = \frac{Q_m K_L C_e}{1 + K_L C_e} \tag{3}$$

$$Q_e = K_F {C_e}^n \tag{4}$$

$$Q_e = B ln(K_T C_e) \tag{5}$$

where Ce is the equilibrium concentration of the adsorbate (mg/L), K_L the Langmuir adsorption constant (L/mg), Qe is the amount of adsorbate adsorbed per unit mass of adsorbent (mg/g) and Qm is the theoretical maximum adsorption capacity (mg/g). n and K_F (L/mg) are Freundlich constants. K_F is defined as an adsorption or distribution

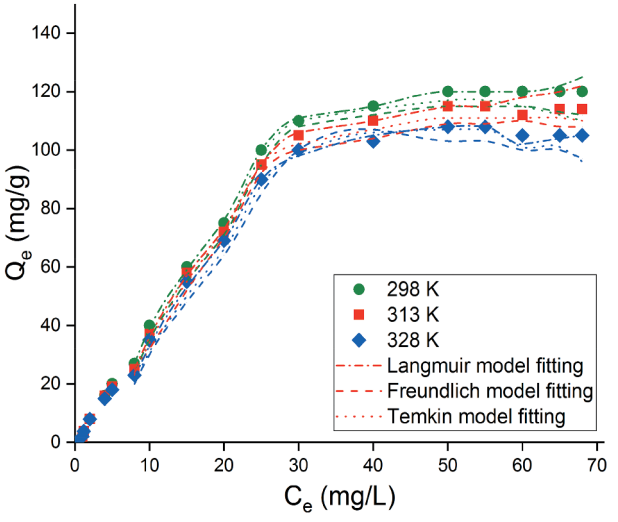

Figure 8. Adsorption isotherm of MO onto the Fe_3O_4-CS adsorbent at different solution temperatures (adsorption conditions: 0.1g/100ml Fe_3O_4-CS, initial MO concentration 2.5–200 mg/L, pH= 3 and 60 min).

coefficient representing the amount of adsorbate adsorbed on an adsorbent for a unit equilibrium concentration while n gives an indication of how favourable the adsorption process. The slope of 1/n ranging between 0 and 1 is a measure of adsorption intensity or surface heterogeneity, becoming more heterogeneous as its value gets closer to zero [51]. B (J/mol) is the Temkin constant related to the heat of adsorption, and K_T (L/mg) is the equilibrium-binding constant. A negative value of B indicates the adsorption process is endothermic, and a positive value of B represents the process is exothermic [52].

The R^2 value of the line drawn according to the Langmuir model for MO adsorption on Fe_3O_4-CS beads at 298 K is closer to 1,000 than the R^2 value obtained according to the Freundlich model (Table 1). Therefore, it can be said that MO adsorption of Fe_3O_4-CS nanocomposite is more suitable for Langmuir model. Also, the values of $n < 1$ indicate that the adsorption process is not suitable for multilayer adsorption. The values of $B > 0$ for all temperatures and can be concluded that the adsorption process is exothermic.

Table 1. Modelling the experimental data of MO adsorption onto the Fe_3O_4-CS adsorbent with the corresponding parameters of the isotherm models.

Model Parameters		Unit	Solution Temperature		
			298 K	313 K	328 K
Langmuir	Q_m	mg/g	132	115	103
	K_L	L/mg	0.058	0.049	0.047
	R^2	_	0.9998	0.9913	0.9874
Freundlich	K_F	$(mg/g)*(mg/L)^n$	4.125	4.018	4.107
	n	_	0.24	0.26	0.22
	R^2	_	0.9214	0.8976	0.9091
Temkin	B	J/mol	201	195	187
	K_T	L/mg	1.052	1.039	1.027
	R^2	_	0.9596	0.9658	0.9579

3.4. Adsorption kinetics

In order to examine the adsorption kinetics of MO on Fe_3O_4-CS beads, non-linear form equations of pseudo-first order (PFO) (Equation 6), pseudo-second order (PSO) (Equation 7) and intra particle diffusion (IPD) kinetic models (Equation 8) were applied.

$$Q_t = Q_e\left(1 - e^{-k_1 t}\right) \tag{6}$$

$$Q_t = \frac{{Q_e}^2 k_2 t}{1 + Q_e k_2 t} \tag{7}$$

$$Q_t = k_{id} t^{1/2} + C \tag{8}$$

The notations Q_e and Q_t express the amount of MO dye adsorbed on Fe_3O_4-CS at equilibrium and a specific time t, while$_1$, k_2 and k_{id} are the pseudo-first, pseudo-second order and intra particle diffusion rate constant, respectively. C is the constant with respect to the boundary layer thickness. The kinetics curves at two initial concentrations of MO adsorption by Fe_3O_4-CS are shown in Figure 9. The corresponding parameters and the correlation coefficients (R^2) of the three models are given in Table 2.

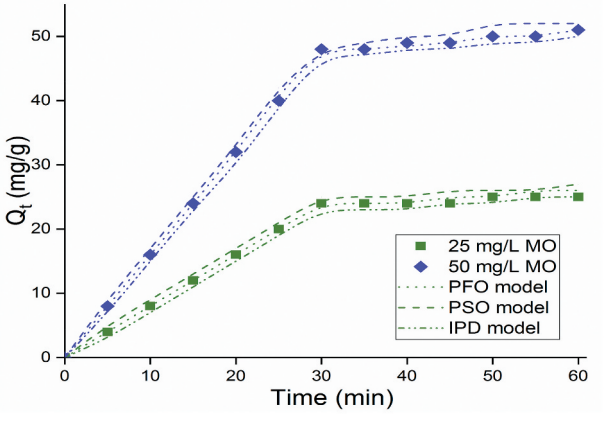

Figure 9. Effect of contact time on the adsorption process of MO onto the Fe_3O_4-CS adsorbent at different initial MO concentrations (adsorption conditions: 0.1g/100ml Fe_3O_4-CS, pH= 3, 298 K).

Table 2. Modelling the experimental data of MO adsorption onto the Fe_3O_4-CS adsorbent with the corresponding parameters of the isotherm models.

Model Parameters		Unit	Initial MO concentration	
			25 mg/L	50 mg/L
PFO	Qe	mg/g	21	40
	k_1	min^{-1}	0.0049	0.0054
	R^2	_	0.9368	0.9471
PSO	Qe	mg/g	23	47
	k_2	g/(mg*min)	0.00053	0.00016
	R^2	_	0.9992	0.9996
IPD	C	mg/g	7.19	8.75
	k_{id}	$(mg/g)*min^{1/2}$	2.571	3.226
	R^2	_	0.8651	0.8876

According to these data, the closest correlation value to 1 is corresponding to pseudo-second order kinetics. Therefore, the Fe_3O_4-CS nanocomposite is more suitable for pseudo-second order kinetics.

3.5. Adsorption thermodynamics

The enthalpy change, entropy change, free energy change and equilibrium constant during adsorption are determined at three different temperatures (298 K, 313 K and 328 K) and the adsorption phenomenon is investigated thermodynamically [53]. The standard free energy of adsorption ΔG°, its standard entropy ΔS°, and its standard enthalpy ΔH° are calculated from the van't Hoff equation [Equation 9–11] shown in Table 3 using the thermodynamic equilibrium constant (K_C, dimensionless) values obtained at various temperatures based on the Langmuir constant (K_L). To overcome the unit problem, all concentrations were changed to molar form based on the standard state C° = 1 mol/L and the K_C values (unitless) were calculated by using Equation 12 [24].

$$\Delta G0 = -RT \ln KC \tag{9}$$

$$lnK_C = \left(\frac{-\Delta H^0}{R}\right)\frac{1}{T} + \frac{\Delta S^0}{R} \tag{10}$$

$$\Delta G^\circ = \Delta \mathrm{H}^\circ - T\Delta S^\circ \tag{11}$$

$$KC \approx KL \times MMO \times C^\circ \times \left(10^3\right) \tag{12}$$

where R is the ideal gas constant (R = 8.314 J/molK), K_C represents the equilibrium constant (dimensionless), T is the absolute temperature (K), K_L (L/mg) is the Langmuir constant; M_{MO} (g/mol) is the methyl orange molar mass; and C° is the standard state (C° = 1 mol/L); the 10^3 factor allows converting the unit from gram to milligram.

The negative ΔG° value of MO adsorption on Fe_3O_4-CS beads indicated that the adsorption occurred spontaneously between 298K and 328K, and the negative ΔH° value indicated that the adsorption was exothermic. In addition, it is seen in Figure 7(e) that the Qe values decreased as the temperature increased. The size of the adsorption enthalpy gives information about the type of adsorption. A positive ΔS° value indicates that the disorder increases during adsorption. The reason for the increase in disorder can be attributed to the removal of water molecules from the adsorbent during the adsorption of the dyestuff onto the adsorbent surface surrounded by a hydrated shell, thus increasing entropy [53].

Table 3. Thermodynamic parameters of the adsorption of MO by Fe_3O_4-CS adsorbent.

ΔG^0 (kJ mol^{-1})			Van't Hoff Equation	ΔH^0 (kJ mol^{-1})	ΔS^0 (J mol^{-1} K^{-1})
298 K	313 K	328 K	y= 1425.31x + 4.97	−11.85	41.31
−24.16	−24.78	−25.39	R^2 = 0.9419		

3.6. Catalytic activity in the CWPO of MO

The degradation of CWPO catalysed by 100 mg Fe_3O_4NPs, Fe_3O_4-CS and Fe_3O_4-AT magnetic nanoparticles of 25 ppm 100 mL MO at pH = 5 at room temperature was investigated, and the results are given in Figure 10. Optimisation studies were carried out with Fe_3O_4-CS, which provides the highest dye removal in the shortest time, and the oxidation reaction kinetics were investigated. When the results performed with Fe_3O_4-CS catalysis at pH = 3, 5, 8 and 10 are investigated at Figure 11(c), it is seen that the best result is obtained at pH = 3 and the colour removal efficiency decreases with increasing basicity. The reason for this is that the oxidation potential of ·OH decreases in the increasing pH [54,55]. In the CWPO experiments conducted at 25°C, 40°C, 55°C and 70°C, the dye removal efficiency was the best achieved at 25°C (Figure 11(d)). From the obtained results, the reaction is considered to be exothermic. In order to understand the effect of H_2O_2 concentration on colour removal efficiency, 20%, 30%, 40% and 50% (v/v) of H_2O_2 solutions were used. It was determined that with the increase of hydrogen peroxide concentration, the decomposition reaction of H_2O_2 to radicals accelerated, and the decomposition of MO increased up to a point and then tended to remain constant (Figure 11(a)). This is because at high concentrations, hydrogen peroxide prevents the formation of hydroxyl radicals, causing the reduction of these radicals [54,56]. In order to examine the effect of the amount of catalyst, experiments were carried out by adding 50, 100, 150 and 250 mg/L of magnetic Fe_3O_4-CS nanocomposite. As can be seen in Figure 11(b), the colour removal efficiency increases with the increase in the amount of catalyst. With the increase in the amount of catalyst, the number of active centres required for oxidation increases, which increases the colour removal efficiency [57,58].

The kinetic studies are very important in catalytic reactions and help to define reaction mechanism and rate in limiting reaction systems. The kinetic studies were carried out at room temperature with 0.05 g Fe_3O_4-CS catalyst and 30% H_2O_2 concentration at pH 3. According to the pseudo-first order kinetic model, ln

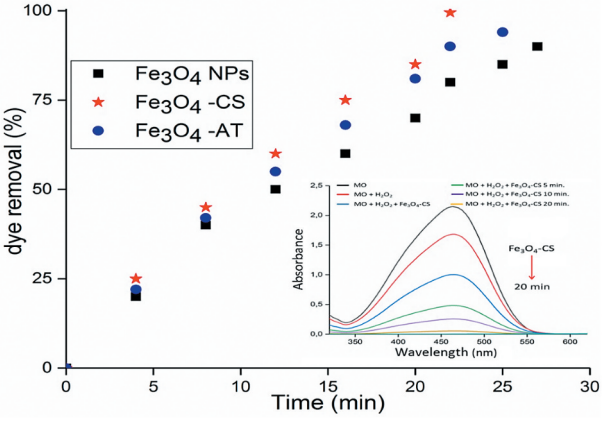

Figure 10. Comparison of the catalytic activity Fe_3O_4NPs, Fe_3O_4-CS and Fe_3O_4-AT for MO in the CWPO (initial dye concentration: 25 mg/L, catalyst dosage= 100mg, pH=5, T = 298 K).

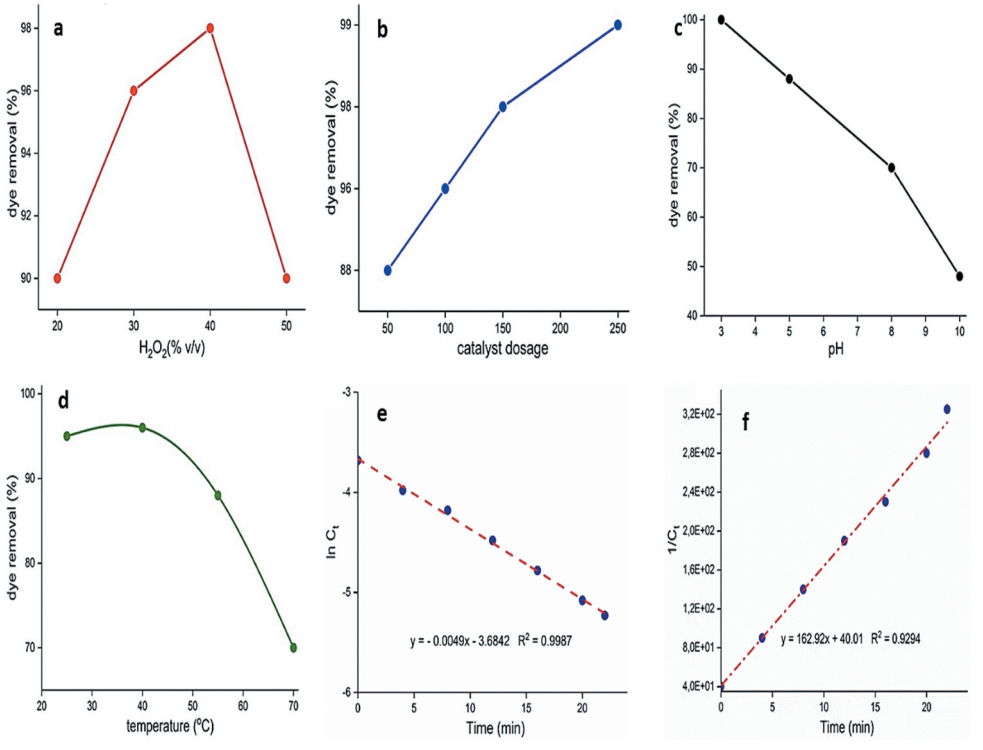

Figure 11. Effect of a) H_2O_2 concentration, b) catalyst dose, c) pH, d) temperature and e) pseudo-first-order, f) pseudo-second-order kinetic models for CWPO of MO on Fe_3O_4-CS.

C values against t were plotted and the k_1 rate constant was determined from the slope. The graph drawn for the pseudo-first order kinetic model is given in Figure 11(c). According to the pseudo-second-order kinetic model, t versus 1/C values were plotted, and the k_2 rate constant was determined from the slope. The graph obtained for the pseudo-second order kinetic model is given in Figure 11(d). The rate constants and R^2 values calculated for pseudo-first-order and pseudo-second-order kinetic models are given in Table 4.

When R^2 values of the two kinetic models are compared, it is seen that the reaction kinetics with a higher R^2 value is compatible with the pseudo-first order kinetic model. From Equation 13, activation energy (E_a) and Arrhenius constant (A) were calculated and found to be 10.72 kJ/mol and 0.40 min^{-1}, respectively.

$$k = Ae^{-Ea/RT} \tag{13}$$

Table 4. Pseudo-first-order and pseudo-second-order model constants for the CWPO of MO by Fe_3O_4-CS catalyst.

Pseudo-first-order		Pseudo-second-order	
k_1 (min^{-1})	R^2	k_2 (g L^{-1} min^{-1})	R^2
0.0049	0.9987	162.92	0.9294

In principle, it can be said that the decompositions of dyes by oxidation are based on the principle of producing OH· radicals. H_2O_2 adsorbed by the metal nanoparticle takes electrons from the metal nanoparticle and forms OH· radicals as a result of OH- ion oxidation. These radicals adsorbed by the nanoparticle react with the dye on the surface and cause the dyes to decompose. In other words, the OH· radical oxidises the dye and converts it to CO_2 and H_2O. The rate of catalytic oxidation depends on both adsorptions of H_2O_2 on the nanoparticle surface and electron transfer from the nanoparticle. It can be said that nanoparticles effectively weaken the O–O bond, providing an advantage for H_2O_2 adsorption and increasing the electron transport rate. In the literature, it has been explained that the possible oxidation reaction mechanism of MO occurs in the presence of hydroxyl (HO•) and hydroperoxyl (HOO•) radicals formed from H_2O_2 [59].

It is important that the heterogeneous catalyst can be used repeatedly in catalytic wet peroxide oxidation systems. Mechanisms such as sintering of metals on the catalyst, dissolution of active components, poisoning of active centres with reagents or by-products, metal oxidation, inactive metal or metal oxide accumulation can cause reductions in the reaction rates and active surface areas of the catalysts. In addition to these, all reaction conditions such as pH, reagents, intermediates and end products play an important role in reducing the activity and selectivity of the catalyst. In order to examine the reusability of the catalyst, the magnetic Fe_3O_4-CS catalyst, which was separated from the solution with a magnet at the end of the experiment, was used again and this process was repeated for three cycles. When the results are examined, it is seen that there is a slight decrease in the removal efficiencies in the 3rd cycle and the stable and active structure of the catalyst is preserved to the desired extent (Dye removal efficiency was observed as 99% in the 1st and 2nd cycle and 97% in the 3rd cycle).

The adsorption capacities of the Fe_3O_4-CS nanoadsorbent are synthesised in this study and the different adsorbents in the literature for the degradation of different dyes are given in Table 5.

Table 5. A comparison of the adsorptive capacity of the prepared sorbent with those announced in the literature.

Dye	Adsorbent	Operating Conditions	Q_m (mg/g)	Reference
MO	Chitosan/diatomite composite	dosage: 200mg/L, contact time: 40 min, 25 ◦C, pH 5	35	[60]
MO	Banana peel Orange peel	dosage: 100 mg/L, contact time: 24 h, 30 ◦C, 180 rpm, pH 6–7	21 20.5	[61]
MO	Chitosan/organic rectorite-Fe_3O_4	dosage: 40 mg/L contact time: 80 min, 25 ◦C, 200 rpm, pH 3	5.56	[62]
MO	Polypyrrole/chitosan	dosage: 100 mg/L contact time: 40 min, 25 ◦C, 200 rpm, pH 4.5	95	[63]
MB	Banana peel	dosage: 100 mg/L, contact time: 24 h, 30 ◦C, 180 rpm, pH 6–7	20.8	[61]
CR	Orange peel	dosage: 100 mg/L, contact time: 24 h, 30 ◦C, 180 rpm, pH 6–7	14	[61]
MO	Fe_3O_4NPs	dosage: 0.1g/100mL contact time:60 min, 25 ◦C, 250 rpm, pH 3	132	Present Study

4. Conclusion

Magnetic nanoparticles and nanocomposites (Fe_3O_4NPs, Fe_3O_4-CS and Fe_3O_4-AT) were synthesised using endemic plant extract with an economical, environmentally friendly and economically green method. Characterisations of synthesised magnetic nanoparticles (MNPs) were performed. Furthermore, their use as adsorbent and catalyst in the removal of MO dye from wastewater was investigated. Optimum conditions were determined for dye removal with the highest efficiency in the shortest time. In addition, kinetic, isotherm and thermodynamic studies were carried out. While the dye removal was successfully performed with Fe_3O_4NPs, Fe_3O_4-CS and Fe_3O_4-AT in both CWPO and adsorption studies, the highest removal efficiency in the shortest time was obtained with Fe_3O_4-CS. Ninety-nine per cent of MO removal efficiency was achieved with Fe_3O_4-CS at 8 min and 20 min for adsorption and CWPO technique, respectively.

Disclosure statement

No potential conflict of interest was reported by the author(s).

ORCID

Muradiye Şahin http://orcid.org/0000-0002-5445-6682
Yasin Arslan http://orcid.org/0000-0002-3743-5679
Fatma Tomul http://orcid.org/0000-0001-6771-3943

References

[1] Q. Yin, L. Tan, Q. Lang, X. Ke, L. Bai, K. Guo, R. Qiao and S. Bai, Appl. Catal. B: Environ **224**, 671 (2018). doi:10.1016/j.apcatb.2017.11.024.
[2] Y. Zhu, M. Ramasamy and D.K. Yi, ACS Appl. Mater. Interfaces **6**, 15078 (2014). doi:10.1021/am503153v.
[3] L.A. Austin, M.A. Mackey, E.C. Dreaden and M.A. El-Sayed, Arch. Toxicol. **88**, 1391 (2014). doi:10.1007/s00204-014-1245-3.
[4] M. Sundararajan, L.J. Kennedy, P. Nithya, J.J. Vijaya and M. Bououdina, J. Phys. Chem. Solids. **108**, 61 (2017). doi:10.1016/j.jpcs.2017.04.002.
[5] R.K. Gautam, P.K. Gautam, S. Banerjee, S. Soni, S.K. Singh and M.C. Chattopadhyaya, J. Mol. Liq. **204**, 60 (2015). doi:10.1016/j.molliq.2015.01.038.
[6] J.H. Kim, S.M. Kim, Y.I. Kim and J. Nanosci, Nanotechnol **14**, 8739 (2014). doi:10.1166/jnn.2014.9993.
[7] F.X. Redl, C.T. Black, G.C. Papaefthymiou, R.L. Sandstrom, M. Yin, H. Zeng, C.B. Murray and S. P. O'Brien, J. Am. Chem. Soc. **126**, 14583 (2004). doi:10.1021/ja046808r.
[8] J. Park, K. An, Y. Hwang, J.G. Park, H.J. Noh, J.Y. Kim, J.H. Park, N.M. Hwang and T. Hyeon, Nat. Mater. **3**, 891 (2004). doi:10.1038/nmat1251.
[9] A. Tavakoli, M. Sohrabi and A. Kargari, Chem. Pap **61**, 151 (2007). doi:10.2478/s11696-007-0014-7.
[10] X. Wang, J. Zhuang, Q. Peng and Y. Li, Nature **437**, 121 (2005). doi:10.1038/nature03968.
[11] S. Babel and T.A. Kurniawan, J. Hazard. Mater **97**, 219 (2003). doi:10.1016/S0304-3894(02)00263-7.
[12] P. Karpagavinayagam, and C. Vedhi, Vacuum **160**, 286 (2019). doi:10.1016/j.vacuum.2018.11.043.

[13] Y. Yi, G. Tu, P.E. Tsang, S. Xiao and Z. Fang, Mater. Lett. **234**, 388 (2019). doi:10.1016/j.matlet.2018.09.137.
[14] L. Liu, M. Bilal, X. Duan and H.M.N. Iqbal, Sci. Total Environ. **667**, 444 (2019). doi:10.1016/j.scitotenv.2019.02.390.
[15] E. Haque, J.W. Jun and S.H. Jhung, J. Hazard. Mater. **185**, 507 (2011). doi:10.1016/j.jhazmat.2010.09.035.
[16] D. Yaseen, and M. Scholz, Int. J. Environ. Sci. Technol **16**, 1193 (2019). doi:10.1007/s13762-018-2130-z.
[17] V. Katheresan, J. Kansedo and S.Y. Lau, J. Environ. Chem. Eng **6**, 4676 (2018). doi:10.1016/j.jece.2018.06.060.
[18] M. Solís, A. Solís, H.I. Pérez, N. Manjarrez and M. Flores, Process. Biochem. **47**, 1723 (2012). doi:10.1016/j.procbio.2012.08.014.
[19] M.S. Khehra, H.S. Saini, D.K. Sharma, B.S. Chadha and S.S. Chimni, Dyes Pigm. **70**, 1 (2006). doi:10.1016/j.dyepig.2004.12.021.
[20] R.L. Singh, P.K. Singh and R.P. Singh, Int. Biodeterior. Biodegradation **104**, 21 (2015). doi:10.1016/j.ibiod.2015.04.027.
[21] U. Shanker, M. Rani and V. Jassal, Environ. Chem. Lett. **15**, 623 (2017). doi:10.1007/s10311-017-0650-2.
[22] K. Nithya, A. Sathish, P.S. Kumar and T. Ramachandran, J. Ind. Eng. Chem **59**, 230 (2018). doi:10.1016/j.jiec.2017.10.028.
[23] S.H. Lee, H. Choi and K.W. Kim, J. Geochem. Explor. **184**, 247 (2018). doi:10.1016/j.gexplo.2016.11.015.
[24] F. Tomul, Y. Arslan, B. Kabak, D. Trak, E. Kendüzler, E.C. Lima and H.N. Tran, Sci. Total Environ. **726**, 137828 (2020). doi:10.1016/j.scitotenv.2020.137828.
[25] M. Sahin, and I.H. Gubbuk, React. Kinet. Mech. Catal **135**, 999 (2022). doi:10.1007/s11144-022-02185-y.
[26] B. Baruwati, and R.S. Varma, Chem Suschem. **2**, 1041 (2009). doi:10.1002/cssc.200900220.
[27] H. Baseri, and S. Tizro, Process Saf. Environ. Prot **109**, 465 (2017). doi:10.1016/j.psep.2017.04.022.
[28] V. Thamilarasan, V. Sethuraman, K. Gopinath, C. Balalakshmi, M. Govindarajan, R.A. Mothana, N.A. Siddiqui, J.M. Khaled and G. Benelli, J. Clust. Sci **29**, 375 (2018). doi:10.1007/s10876-018-1342-1.
[29] M. Kumari, C.U. Pittman Jr and D. Mohan, J. Colloid Interface Sci. **442**, 120 (2015). doi:10.1016/j.jcis.2014.09.012.
[30] C. Yuwei, and W. Jianlong, Chem. Eng. J **168**, 286 (2011). doi:10.1016/j.cej.2011.01.006.
[31] A. Azizi, J. Inorg. Organomet. Polym **30**, 3552 (2020). doi:10.1007/s10904-020-01500-1.
[32] S. Hussain, M. Kamran, S.A. Khan, K. Shaheen, Z. Shah, H. Suo, Q. Khan, A.B. Shah, W. U. Rehman, Y.O. Al-Ghamdi and U. Ghani, Int. J. Biol. Macromol. **168**, 383 (2021). doi:10.1016/j.ijbiomac.2020.12.054.
[33] N. Illy, M. Robitzer, R. Auvergne, S. Caillol, G. David and B. Boutevin, J. Polym. Sci. A Polym. Chem. **52**, 39 (2013). doi:10.1002/pola.26967.
[34] A. Mohammadi, H. Daemi and M. Barikani, Int. J. Biol. Macromol. **69**, 447 (2014). doi:10.1016/j.ijbiomac.2014.05.042.
[35] Z. Ayazi, Z.M. Khoshhesab, F.F. Azhar and Z. Mohajeri, J. Chin. Chem. Soc **64**, 627 (2017). doi:10.1002/jccs.201600876.
[36] L. Yang, X. Ma and N. Guo, Carbohydr. Polym. **90**, 853 (2012). doi:10.1016/j.carbpol.2012.06.011.
[37] M. Yamaura, R.L. Camilo, L.C. Sampaio, M.A. Macedo, M. Nakamura and H.E. Toma, J. Magn. Magn. Mater. **279**, 210 (2004). doi:10.1016/j.jmmm.2004.01.094.
[38] X.R. Ye, C. Daraio, C. Wang, J.B. Talbot and S. Jin, J. Nanosci. Nanotechnol. **6**, 852 (2006). doi:10.1166/jnn.2006.135.
[39] G. Li, K. Huang, Y. Jiang, P. Ding and D. Yang, Biochem. Eng. J. **40**, 408 (2008). doi:10.1016/j.bej.2008.01.018.

[40] G. Li, Y. Jiang, K. Huang, P. Ding and J. Chen, J. Alloys Compd. **466**, 451 (2008). doi:10.1016/j.jallcom.2007.11.100.
[41] N.S.A. Mubarak, T.W. Chuan, H.P. Khor, A.H. Jawad, L.D. Wilson and S. Sabar, J. Polym. Environ **29**, 1050 (2021). doi:10.1007/s10924-020-01949-8.
[42] A. Shameem, P. Devendran, V. Siva, K.S. Venkatesh, A. Manikandan, S.A. Bahadur and N. Nallamuthu, J. Inorg. Organomet. Polym. Mater. **28**, 671 (2018). doi:10.1007/s10904-017-0710-x.
[43] M. Kragović, M. Stojmenović, J. Petrović, J. Loredo, S. Pašalić, A. Nedeljković and I. Ristović, Procedia. Manuf. **32**, 286 (2019). doi:10.1016/j.promfg.2019.02.216.
[44] Z. Anfar, M. Zbair, H.A. Ahsaine, Y. Abdellaoui, A.A.E. Fakir, E.H. Ameterz, A. Jada and N.E. Alem, Chem. Select **4**, 4981 (2019). doi:10.1002/slct.201901043.
[45] H. Haffad, M. Zbair, Z. Anfar, H.A. Ahsaine, H. Bouhlal and H. Khallok, Toxin. Rev. **2**, 225 (2021). doi:10.1080/15569543.2019.1584822.
[46] Z. Anfar, A. Amedlous, A.A.E. Fakir, H.A. Ahsaine, M. Zbair, S. Lhanafi, R.E. Haouti, A. Jada and N. E. Alem, ACS Omega. **4**, 9434 (2019). doi:10.1021/acsomega.9b00524.
[47] N. Quasfi, S. Bouzekri, M. Zbair, H.A. Ahsaine, S. Bakkas, M. Bensitel and L. Khamliche, Surf. Interfaces. **14**, 61 (2019). doi:10.1016/j.surfin.2018.11.008.
[48] P. Baskaralingam, M. Pulikesi, V. Ramamurthi and S. Sivanesan, Appl. Clay. Sci. **37**, 207 (2007). doi:10.1016/j.clay.2007.01.014.
[49] K. Chen, J. He, Y. Li, X. Cai, K. Zhang, T. Liu, Y. Hu, D. Lin, L. Kong and J. Liu, J. Colloid Interface Sci. **494**, 307 (2017). doi:10.1016/j.jcis.2017.01.082.
[50] L. Fan, Y. Zhang, X. Li, C. Luo, F. Lu and H. Qiu, Colloids Surf. B Biointerfaces. **91**, 250 (2012). doi:10.1016/j.colsurfb.2011.11.014.
[51] K. Fytianos, E. Voudrias and E. Kokkalis, Chemosphere **40**, 3 (2000). doi:10.1016/S0045-6535(99)00214-3.
[52] P. Paluri, K.A. Ahmad and K.S. Durbha, Biomass Conv. Bioref **12**, 4031 (2020). doi:10.1007/s13399-020-00867-y.
[53] K.Z. Elwakeel, J. Hazard. Mater **167**, 383 (2009). doi:10.1016/j.jhazmat.2009.01.051.
[54] X. Shi, A. Tian, J. You, H. Yang, Y. Wang and X. Xue, J. Hazard. Mater. **353**, 182 (2018). doi:10.1016/j.jhazmat.2018.04.018.
[55] K. Chellal, K. Bachari and F. Sadi, J. Clust. Sci **25**, 523 (2014). doi:10.1007/s10876-013-0632-x.
[56] R. Saleh, and A. Taufik, Sep. Purif. Technol. **210**, 563 (2019). doi:10.1016/j.seppur.2018.08.030.
[57] J.H. Park, J.J. Wang, R. Xiao, N. Tafti, R.D. Delaune and D.C. Seo, Bioresour. Technol. **249**, 368 (2018). doi:10.1016/j.biortech.2017.10.030.
[58] K.K. Rubeena, P.H.P. Reddy, A.R. Laiju and P.V. Nidheesh, J. Environ. Manage. **226**, 320 (2018). doi:10.1016/j.jenvman.2018.08.055.
[59] J. Han, H.Y. Zeng, S. Xu, C.R. Chen and X.J. Liu, Appl. Catal. A Gen **527**, 72 (2016). doi:10.1016/j.apcata.2016.08.015.
[60] P. Zhao, R. Zhang and J. Wang, Water Sci. Technol. **75**, 1633 (2017). doi:10.2166/wst.2017.034.
[61] G. Annadurai, R.S. Juang and D.J. Lee J. Hazard. Mater **92**, 263 (2002). doi:10.1016/S0304-3894(02)00017-1.
[62] L. Zeng, M. Xie, Q. Zhang, Y. Kang, X. Guo, H. Xiao, Y. Peng and J. Luo, Carbohydr. Polym. **123**, 89 (2015). doi:10.1016/j.carbpol.2015.01.021.
[63] N.S. Alsaiari, A. Amari, K.M. Katubi, F.M. Alzahrani, F.B. Rebah and M.A. Tahoon, Processes **9**, 576 (2021). doi:10.3390/pr9040576.